

Breaking the Ice: Exploring the Changing Dynamics of Winter Breakup Events in the Beaufort Sea

Jonathan W. Rheinlænder^{1,2}, Heather Regan¹, Pierre Rampal^{3,1}, Guillaume
Boutin¹, Einar Ólason¹, Richard Davy¹

¹Nansen Environmental and Remote Sensing Center and Bjerknes Centre for Climate Research, Bergen,
Norway

²Department of Earth Science, University of Bergen, and Bjerknes Centre for Climate Research, Bergen,
Norway

³Centre National de la Recherche Scientifique, Institut de Géophysique de l'Environnement, Grenoble,
France

Key Points:

- Modelled leads in the Beaufort Sea during wintertime are increasing at 4% per decade over the period 2000-2018
- The shift to thinner and younger sea ice, particularly after 2007, makes the Beaufort Sea more vulnerable to large breakup events by winds
- Winter breakup increases ice export from the Beaufort Sea and leads to a thinner and weaker ice cover at the end of the cool season

Corresponding author: Jonathan W. Rheinlænder, jonathan.rheinlaender@nersc.no

Abstract

The Beaufort Sea has experienced a significant decline in sea ice, with thinner first-year ice replacing thicker multi-year ice. This transition makes the ice cover weaker and more mobile, making it more vulnerable to breakup during winter. Using a coupled ocean-sea-ice model, we investigated the impact of these changes on sea-ice breakup events and lead formation from 2000 to 2018. The simulation shows an increasing trend in the Beaufort Sea lead area fraction during winter, with a pronounced transition around 2007. A high lead area fraction in winter promotes a significant growth of new, thin ice within the Beaufort region while also leading to enhanced sea ice transport out of the area. The export offsets ice growth, resulting in negative volume anomalies and preconditioning a thinner and weaker ice pack at the end of the cool season. Our results indicate that large breakup events may become more frequent as the sea-ice cover thins and that such events only became common after 2007. This result highlights the need to represent these processes in global-scale climate models to improve projections of the Arctic.

Plain Language Summary

The sea ice cover in the Beaufort Sea has been changing - it is getting thinner and weaker. This makes the ice more likely to break apart from strong winds. Using a computer model, we study how these changes may have affected the frequency of large sea-ice breakup events from 2000 to 2018. We find that the amount of open areas in the sea ice, called leads, is increasing during winter. This allows new, thin ice to form, but also causes more ice to move out of the region under the action of winds and currents. This movement of ice cancels the growth of new ice, resulting in less ice overall at the end of winter in this region. Interestingly, these events became more common after 2007 and the results suggests that bigger breakup events might happen more often as the sea ice continues to thin. This study highlights how important it is to include these changes in large climate models to better predict what might happen in the Arctic in the future.

1 Introduction

Recent decades have seen dramatic reductions in the extent, age, and thickness of Arctic sea ice (e.g. Kwok, 2018). Those changes are particularly pronounced in the Beaufort Sea, which has experienced a rapid decline in sea ice extent and sea ice thickness, during both summer and winter. There has been a notable shift in the composition of

49 sea ice in the early-2000s (Babb et al., 2022), where the Beaufort ice cover transitioned
50 from a state which was dominated by thick and old multi-year ice (MYI) to an increas-
51 ingly thinner, more fragmented and mobile seasonal ice cover around 2007 (Moore et al.,
52 2022; Wood et al., 2013). This regime shift towards younger, thinner sea ice is affect-
53 ing the dynamical properties of the ice cover (Zhang et al., 2012), reducing the ice’s me-
54 chanical strength, thereby making it more vulnerable to atmospheric forcing (Petty et
55 al., 2016) and contributing to the observed increase in sea ice deformation and drift speeds
56 in the Arctic Ocean and the Beaufort Sea in particular (Rampal et al., 2009; Kwok &
57 Cunningham, 2010; Spreen et al., 2011). These changes in sea ice properties and ice dy-
58 namics have consequences for the stability and persistence of the Beaufort Sea ice cover,
59 potentially resulting in more frequent sea ice breakup and lead formation (Maslanik et
60 al., 2007). This potentially has important implications for the overall mass balance of
61 sea ice, ice-ocean interactions, and the Arctic climate system. However, due to the lack
62 of long-term observations and the difficulties in modelling sea-ice breakup, our knowl-
63 edge is currently limited when it comes to understanding the relationship between these
64 changing sea ice characteristics and the frequency and intensity of breakup events.

65 During winter months, lead formation exposes the ocean to the colder atmosphere
66 resulting in large air-sea heat, moisture and gas fluxes. The intense heat loss from the
67 ocean promotes new ice formation, contributing to the sea ice mass balance in the Arc-
68 tic winter (accounting for between 10 and 20% of the total ice growth in the Arctic dur-
69 ing winter Heil & Hibler, 2002; Kwok, 2006). Recent estimates from Boutin et al. (2023)
70 show that this number could be as high as 25–35%. Brine rejection from sea ice forma-
71 tion increases the stability of the Arctic halocline (Shimada et al., 2005), which protects
72 sea ice from melting by suppressing the entrainment of subsurface heat into the surface
73 layer. Brine-driven eddies under sea ice leads can affect thermohaline structure of the
74 mixed layer by transporting heat and salt laterally under the sea ice (Matsumura & Ha-
75 sumi, 2008; Peralta-Ferriz & Woodgate, 2015). Leads are also key regions for marine bi-
76 ological productivity due to increased access to sunlight, which is otherwise very limited
77 due to the presence of thick, snow-covered sea ice. For example, recent observations show
78 that leads in Arctic pack ice can enable early phytoplanktonic blooms (Assmy et al., 2017)
79 impacting primary production and Arctic marine food webs. This could become more
80 frequent due to thinner and more dynamic sea ice that is more vulnerable to breakup
81 (Fadeev et al., 2021).

82 In the Beaufort Sea, leads regularly form throughout the winter season in response
83 to divergent sea ice motion driven by atmospheric weather systems or ocean currents (Lewis
84 & Hutchings, 2019; Jewell & Hutchings, 2023). Meanwhile, several large breakup events
85 have been identified from satellite observations in recent decades (most noteworthy in
86 the winters of 2013 (Beitsch et al., 2014; Rheinländer et al., 2022) and 2016 (Babb et
87 al., 2019)). Wintertime breakup events are characterized by extensive fracturing of the
88 ice cover associated with atmospheric synoptic conditions persisting from a few days to
89 several weeks (Jewell & Hutchings, 2023). Such events have been shown to significantly
90 impact sea ice conditions in the Beaufort Sea, with potential implications for the wider
91 Arctic sea ice mass balance. The large breakup events in winter 2013 and 2016 resulted
92 in anomalous sea ice drift and enhanced ice export out of the Beaufort Sea (e.g. Babb
93 et al., 2016; Rheinländer et al., 2022). This led to an overall reduction in the Beaufort
94 ice volume in April and a thinner, less compact ice cover prior to the onset of the melt-
95 ing season. This conditions the ice cover for rapid summer melt (e.g. Maslanik et al.,
96 2007) and could contribute to the low regional September sea ice area seen in recent decades
97 (Williams et al., 2016; Babb et al., 2019; Moore et al., 2022).

98 Winter breakup events can also have important consequences for the MYI cover.
99 Enhanced ice export during winter may increase the flushing of MYI through the Beau-
100 fort Sea which increases the amount of MYI being advected into the region from the cen-
101 tral Arctic (as was seen in 2013, e.g. Richter-Menge & Farrell, 2013). This could mo-
102 bilize the oldest and thickest sea ice residing north of Greenland, also known as the Last
103 Ice Area, which is subsequently advected into the Beaufort Sea. For example, during sum-
104 mer 2020/21 Moore et al. (2022) found large concentrations of thick and old ice in the
105 Beaufort Sea, which could be traced back to enhanced winter transport from the Last
106 Ice Area. Less MYI now survives through the summer melt season, making the Beau-
107 fort Sea a major contributor to MYI loss in the Arctic (Howell et al., 2016; Babb et al.,
108 2022).

109 Despite their importance, sea ice breakup and lead formation are generally not ad-
110 equately reproduced in large-scale sea-ice and climate models (e.g. Spreen et al., 2017).
111 This is partly due to the difficulty in representing small-scale deformation features, like
112 cracks and leads, for horizontal resolutions coarser than ~ 5 km (Hutter et al., 2022). And
113 while higher resolution sea-ice models (4–5 km) have demonstrated a certain degree of
114 proficiency in representing the large-scale distribution of sea-ice leads in the Arctic (e.g.

115 Wang et al., 2016), they are currently considered too costly for global-scale climate mod-
116 els.

117 In this study we present a newly developed coupled ocean-sea ice model based on
118 the neXtSIM sea-ice model which employs a brittle sea-ice rheology making it partic-
119 ularly suitable for simulating small-scale ice deformation and linear kinematic features
120 like fractures and leads in sea ice at comparatively low resolution (about 12 km here)
121 (Rampal et al., 2019; Bouchat et al., 2022; Ólason et al., 2022). Rheinländer et al. (2022)
122 recently demonstrated neXtSIM’s ability to provide a realistic and accurate represen-
123 tation of sea ice fracturing and lead propagation associated with the 2013 breakup event
124 in the Beaufort Sea. The study highlighted that such extreme breakup events could be-
125 come more frequent as the sea ice thins, raising concerns about the vulnerability of the
126 Beaufort ice cover. Here, we seek to understand how changes in the Beaufort sea-ice regime
127 during the early 21st century have affected the stability of the ice cover and the occur-
128 rence of extreme breakup events focusing on the winters of 2000–2018. By addressing
129 this question, this study aims to provide new insights into the ongoing transformations
130 of the Beaufort Sea ice cover and its implications for regional sea ice volume, MYI cov-
131 erage, and sea-ice transport.

132 2 Methods

133 2.1 Model setup

134 The model used in this study is the new coupled sea-ice-ocean model recently pre-
135 sented in Boutin et al. (2023). In brief, the ocean component is the Océan PARallélisé
136 model (OPA), which is part of the NEMO3.6 modelling platform (Madec, 2008). We use
137 the regional CREG025 configuration (Talandier & Lique, 2021), which encompasses the
138 Arctic and parts of the North Atlantic down to 27°N, and has 75 vertical levels and a
139 nominal horizontal resolution of $1/4^\circ$ ($\simeq 12$ km in the Arctic basin). The sea ice com-
140 ponent is neXtSIM, a state-of-the-art, finite element, sea ice model using a moving La-
141 grangian mesh (Bouillon & Rampal, 2015; Rampal et al., 2016). Sea ice dynamics rely
142 on the Brittle Bingham-Maxwell (BBM) rheology described in Ólason et al. (2022), while
143 sea ice thermodynamics are simulated following the Winton (2000) model. We refer to
144 Boutin et al. (2023) for detailed information about the model setup.

145 As noted by Hutter et al. (2022), sea ice models generally struggle to simulate sea
 146 ice dynamics when run at resolutions coarser than about 5 km; in particular, features
 147 like fractures, shear zones, and lead openings. However, the BBM rheology has demon-
 148 strated its capability to reproduce deformations consistent with observations when run-
 149 ning at a resolution of $O(10\text{ km})$ in the neXtSIM model (Ólason et al., 2022) and in the
 150 SI3 model (L. Brodeau, personal communication). Specifically, these models exhibit ex-
 151 cellent capability in accurately capturing the divergence rates associated with the open-
 152 ing of leads when using the BBM rheology (Ólason et al., 2022; Rheinländer et al., 2022).

153 The simulation presented in this study is the same as in Regan et al. (2023) and
 154 Boutin et al. (2023). The simulation starts in 1995 and ends in 2018. The first five years
 155 were considered a spin-up period and disregarded for analysis. Atmospheric forcing is
 156 taken from the hourly ERA5 reanalysis at a $1/4$ -degree horizontal resolution. This sim-
 157 ulation has been thoroughly evaluated in two recent publications (Boutin et al., 2023;
 158 Regan et al., 2023). Boutin et al. (2023) showed that simulating key sea-ice quantities
 159 like volume, extent, large-scale drift, and sea ice deformations are consistent with satel-
 160 lite observations. Regan et al. (2023) demonstrated that the simulation successfully re-
 161 produces the spatial distribution and evolution of observed MYI extent. They also found
 162 a good agreement with observed estimates of the regional dynamic and thermodynamic
 163 components of the winter sea ice mass balance from Ricker et al. (2021).

164 2.2 Lead definition

165 neXtSIM uses three ice categories; open water, young ice, and consolidated ice. Newly
 166 formed ice, thinner than h_{\max} (here set to 18 cm), is assigned to the young ice category,
 167 representing the formation and growth of frazil and young ice in open water. Ice in the
 168 young ice category is transferred to the consolidated ice category as its thickness exceeds
 169 h_{\max} (see appendix A of Rampal et al., 2009). In winter, when the Beaufort Sea is fully
 170 ice-covered, lead opening is the only way open water can be exposed to the atmosphere,
 171 and young ice can be formed. Therefore, we assume (as in Rheinländer et al., 2022; Boutin
 172 et al., 2023) that open water and young ice formed in winter are a proxy for the pres-
 173 ence of leads in the model. We use this assumption to estimate the rapid growth of thin,
 174 newly formed ice in open-water and thin ice regions. A grid cell is considered a lead when
 175 the combined fraction of open water and young ice exceeds a critical threshold c_{lim} , thereby
 176 excluding the thicker pack ice. We found that a value of $c_{lim} = 5\%$ gives a reasonable

177 lead distribution. The sensitivity of the simulated lead fraction to the value of c_{lim} is
178 included in the Supplementary Material. The total lead area fraction (LAF) can then
179 be calculated by multiplying the lead fraction with the area of each grid cell. A snap-
180 shot of the simulated sea ice concentration and lead fraction on 25 March 2016 is shown
181 in Fig. 1. Here, leads are clearly identified as areas of open water and newly formed ice,
182 whereas the pack ice is associated with low lead fraction values. The LAF calculated over
183 the Beaufort region for this instance is 21%, which means that 21% of the Beaufort area
184 is covered by leads.

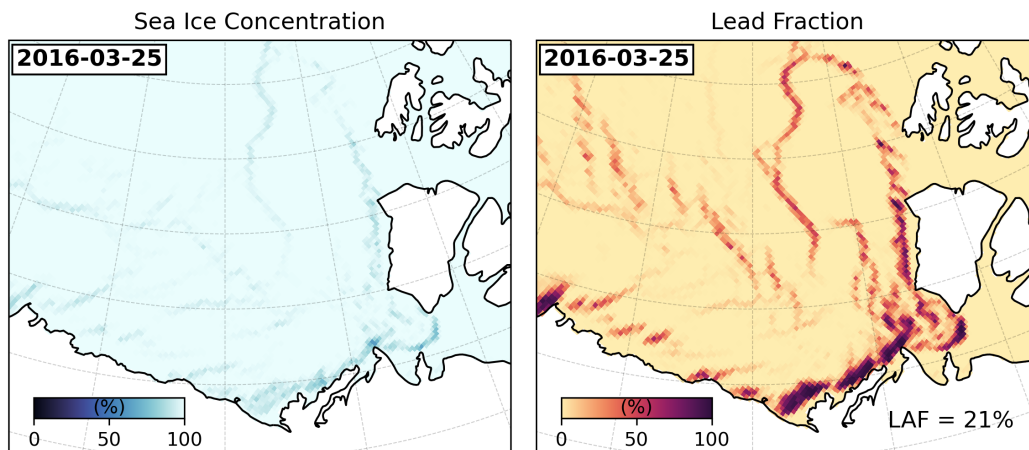


Figure 1. Snapshots of sea ice concentration (%) and lead fraction (%) in the Beaufort Sea on March 25, 2016. The total lead area fraction (LAF) is calculated using a threshold value of 5% (see 2).

3 Results

3.1 Simulated changes in the Beaufort ice cover

Since the 2000s, the MYI extent in the Arctic has declined considerably (Fig. 2a). During the period 2000–2018, the model simulates a decline in the winter MYI area, which is part of a long-term negative trend in the Arctic as seen from satellite observations (e.g. Babb et al., 2022). In the Beaufort Sea region (outlined in Fig. 2a), extensive areas of thicker and older MYI were present during January–March in the early 2000s (i.e. 2000–2004). For the later part of the simulation (years 2014–2018), the MYI extent is significantly reduced and is consistent with the observed trend towards reduced MYI concentration (Howell et al., 2016). Both the average sea ice thickness and MYI concentration computed over the Beaufort region exhibit considerable year-to-year variations (Fig. 2b), but overall there is a shift towards thinner and younger ice types. The average winter sea-ice thickness decreased from 1.9 m in 2000–2004 to 1.6 m in 2014–2018. Meanwhile, some old and thick sea ice still remains located north of Canada and the Last Ice Area, which are important source regions for MYI import to the Beaufort Sea (Moore et al., 2022).

The ice drift speeds in the Beaufort Sea are also increasing (Fig. 2c) with a 12% increase over the 2000–2018 period (not shown). Previously, this increase in ice drift speeds has been linked to thinning of the sea ice cover and enhanced deformation rates leading to more fracturing and lead opening (Rampal et al., 2009). In the following, we examine the impact of transitioning to a more seasonal and thinner ice cover on the formation of leads and sea-ice breakup in the Beaufort Sea.

3.2 Simulated changes in wintertime leads

We show the simulated wintertime LAF in the Beaufort Sea for the period 2000–2018 in Fig. 3. The LAF shows a large day-to-day variability ranging from 5% to 40%, which reflects the intermittent nature of sea-ice fracturing. Winter-mean values (January–March) generally fall between 10% and 25% with a climatological average of 20%. The lead fraction is generally higher in January and decreases during February and March as the ice becomes thicker and more compact (Fig. 3b and c).

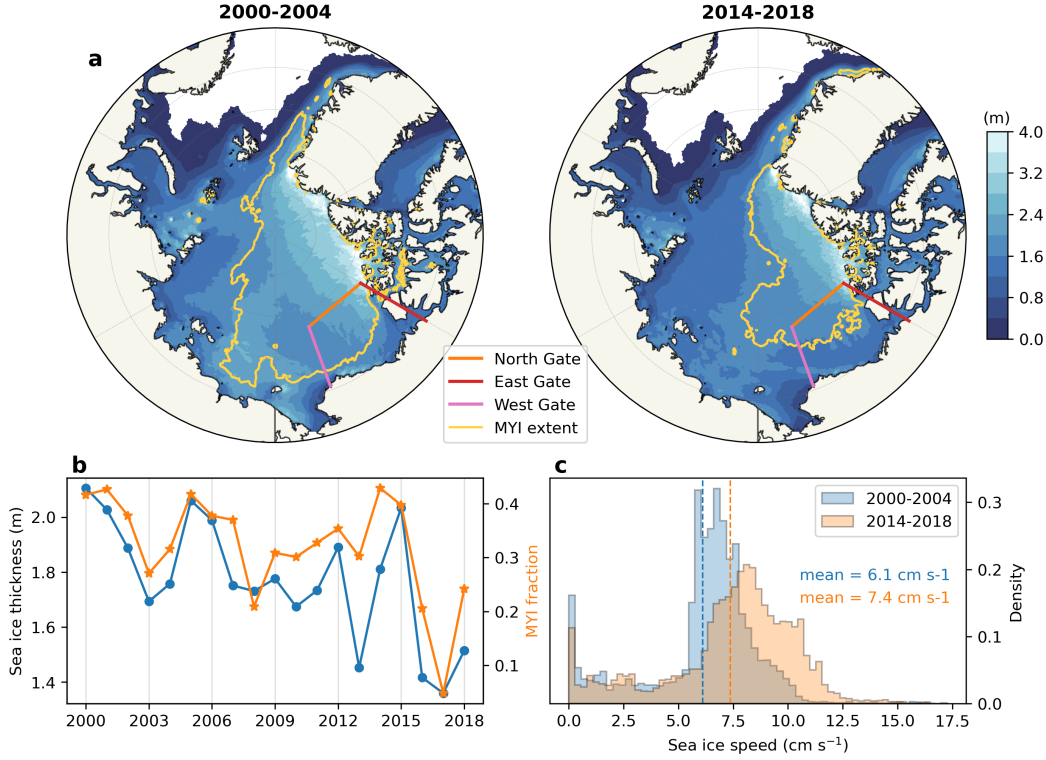


Figure 2. (a) Maps of simulated sea-ice thickness and MYI extent (yellow contour corresponding to the MYI fraction of 0.4) in the Arctic for January–March averaged from 2000–2004 and 2014–2018. (b) Time series of JFM-mean sea-ice thickness and MYI extent averaged in the Beaufort region. (c) Histogram of the winter sea-ice drift speed (cm s^{-1}) distributions for the 2000–2004 and 2014–2018 period. The Beaufort region is bounded by three gates shown in (a); North gate (78°N), East gate (120°W), and West gate (160°W). The definition of the Beaufort region is the same as in Moore et al. (2022).

214 We find a statistically significant increase in wintertime lead occurrences (4.2% per
 215 decade) over the period 2000–2018 based on a simple linear regression analysis (Supple-
 216 mentary Fig. S1). However, the linear relationship becomes less significant when we con-
 217 sider individual months, likely due to the larger spread in the monthly data (Fig. 3b).
 218 Here, we note that the modelled LAF is affected by the cutoff value used in the lead def-
 219 inition (see section 2), but the choice of this cutoff value has no impact on the simulated
 220 variability and trends (Supplementary Fig. S2).

221 The LAF values simulated by neXtSIM are consistent with observations of sea-ice
 222 leads from MODIS at 1 km^2 spatial resolution with observed winter-mean (November–

223 April) lead fraction area ranging between 10–20% in the Beaufort Sea (Willmes et al.,
224 2023). Willmes et al. (2023) also found a significant trend in leads over the 2002–2021
225 period, but only for April. It is worth noting that the MODIS observations have uncer-
226 tainties due to contamination by clouds and will only see opening leads that are rela-
227 tively large. This highlights the need for a dedicated intercomparison study to determine
228 how to best use MODIS imagery to classify and evaluate lead formation in sea-ice mod-
229 els, but this is beyond the scope of this paper.

230 Based on the LAF time series, several larger breakup events can be identified, all
231 occurring after 2007. Most noteworthy are the years 2008, 2010, 2013, 2016, and 2018,
232 which have high average wintertime LAFs (green triangles in Fig. 3a). Many of these
233 events have also been identified in satellite observations (e.g. Jewell & Hutchings, 2023).
234 For example, large breakup events were observed in 2008, 2013 and 2016 and have been
235 described in earlier studies (Wang et al., 2016; Babb et al., 2019; Rheinländer et al., 2022).
236 The breakup being simulated by the model in 2018 is not seen in observations and is likely
237 a result of too strong melting simulated by the model in the summer of 2016 (not shown),
238 leading to thinner sea ice that could break up more easily. During these events, the daily
239 LAF exceeds the 90th percentile (about 30%; Fig. 3c) for a period of more than 15 days
240 during winter (Fig. 3d). We therefore expect these events to have a significant impact
241 on the Beaufort ice cover. Meanwhile, smaller breakup events are also present in other
242 years. For example, 2005 and 2006 exhibit high LAFs (daily values exceeding 35%), but
243 these occurrences are relatively short-lived and result in low winter-mean values over-
244 all. Consequently, they will likely have less impact.

245 Around 2007, we identify a shift in the interannual variability of the LAF based
246 on the monthly values in Fig. 3b. For the 2000–2007 period, the variability (shown by
247 the standard deviation for each month) ranges from 3.1–4.8% during winter. After 2007,
248 this increases to 3.9–7.4% for 2008–2018, and the average LAF increases during all win-
249 ter months. This coincides with more extreme breakups during this period. March, in
250 particular, stands out, showing a 38% increase in the mean LAF relative to the 2000–
251 2007 period while also exhibiting the highest variability (standard deviation of 7.4%).
252 We will investigate this in more detail in section 3.3 and identify some common char-
253 acteristics of the simulated breakup events and their impacts (section 3.4).

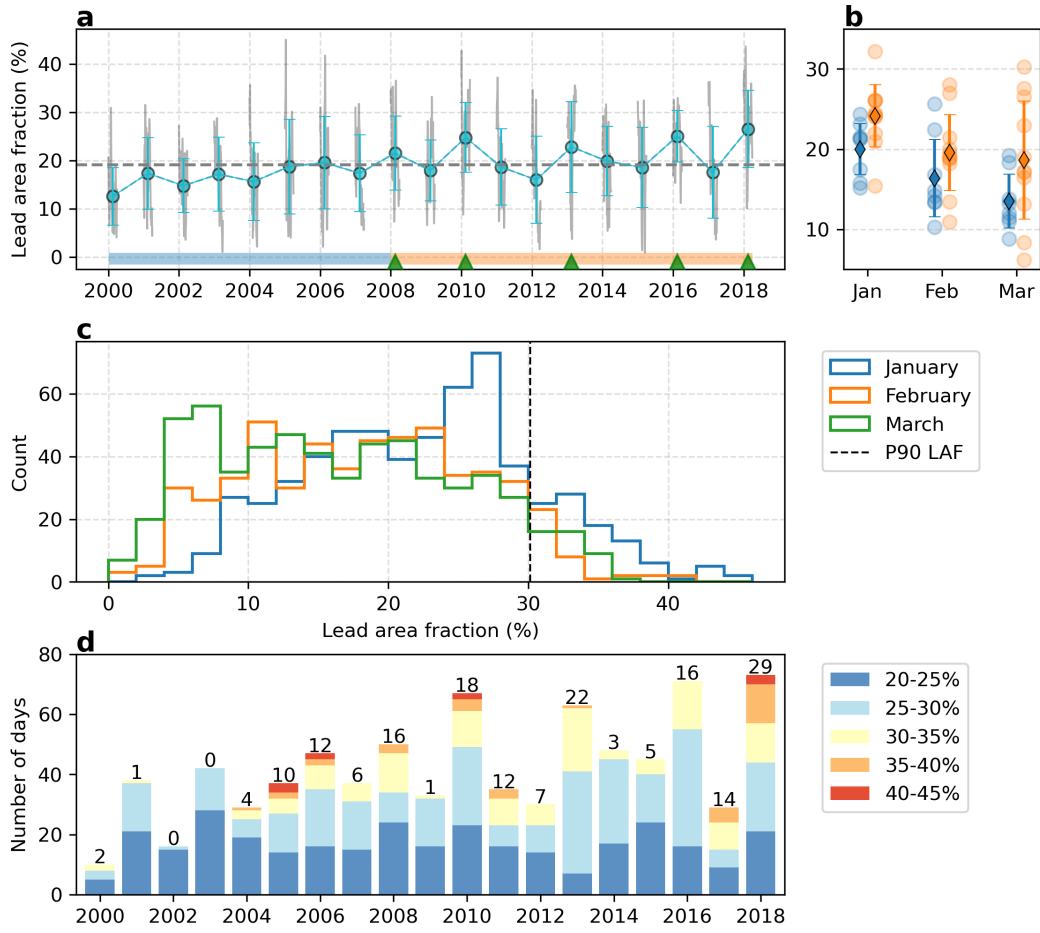


Figure 3. Simulated lead area fraction (LAF; %) in the Beaufort Sea from January through March. (a) Daily LAF (grey) from 2000–2018 with circles showing the winter-mean values along with the standard deviation. The dashed line shows the 2000–2018 winter climatology. (b) Monthly LAF climatologies for the 2000–2007 (blue) and 2008–2018 (orange) periods. Diamonds represent the monthly mean with the standard deviation in whiskers. (c) Histograms of monthly LAF distributions, with the 90th percentile ($\sim 30\%$) shown by the dashed line. (d) Stacked barplot of binned LAF from 20% to 45% where the height of the bars corresponds to the number of days. Numbers denote the total number of days where the daily average LAF exceeds the 90th percentile.

254

3.3 Driving mechanisms of sea-ice breakup events

255

The sea ice movement driven by wind and ocean currents can create stresses within the ice pack, leading to fracturing and the formation of leads (Lewis & Hutchings, 2019).

256

257

In addition, changes in the material properties of the ice, such as ice thickness, concen-

258 tration, and strength, can also influence the susceptibility to breakup. Here we look at
259 the drivers of the simulated changes in winter lead formation, focusing particularly on
260 the shift occurring around 2007.

261 **3.3.1 Winds**

262 Jewell and Hutchings (2023) analysed the synoptic conditions during breakup events
263 in the Beaufort Sea during winters 1993–2013. They show a consistent connection be-
264 tween wind forcing and lead formation, where a breakup is typically associated with high
265 sea level pressure and relatively strong anticyclonic winds over the Beaufort Sea. Sim-
266 ilarly, Wang et al. (2016) concluded that a stronger Beaufort High results in stronger south-
267 easterly winds in the Beaufort Sea, which pushes sea ice away from the coast and thus
268 promotes higher ice divergence and lead formation.

269 In general, high wintertime LAFs in the Beaufort Sea are linked with persistently
270 higher wind speeds (Figure 4b and c) in agreement with Jewell and Hutchings (2023).
271 In 2010, 2013, and 2016, the daily wind speed exceeds 8.5 m s^{-1} (one standard devia-
272 tion above the mean) for more than 20 days (Fig. 4d). These conditions are typically
273 associated with a positive sea level pressure difference across the Beaufort Sea and east-
274 erly winds (Supplementary Fig. S3), creating favourable conditions for off-shore ice drift
275 and enhanced breakup. It is worth noting that there is considerable variability between
276 the different months (Figure 4c and Supplementary Fig. S3), and we do not find a sim-
277 ple relationship between wind speed and sea-ice breakup. Jewell and Hutchings (2023)
278 came to the same conclusion indicating that breakup may occur for a wide range of at-
279 mospheric conditions. Both the duration of strong winds as well as the wind direction
280 appear to be important for initiating a breakup. For example, in 2005, conditions were
281 comparable to other breakup years (e.g. 2013), with relatively strong and persistent winds
282 during winter, however the LAF remained relatively low throughout the winter of 2005
283 (Supplementary Fig. S4). This could be due to the fact that the ice was thicker and stronger
284 (Fig. 2b) and thus less sensitive to winds.

285 We find no trend in the ERA5 winds in the Beaufort region during winter over the
286 period 2000 to 2018 (Fig. 4b). The year-to-year variability is also relatively similar for
287 the 2000–2007 and the 2008–2018 winter periods. The same is true if we consider indi-
288 vidual months rather than the winter-mean values (Fig. 4c), showing no major differ-

289 ence in wind strength for January versus March. Thus, changes in the wind forcing can-
290 not explain the fact that we are seeing the strongest increase in lead variability in March.
291 Based on this, we speculate that the shift in the lead formation dynamics seen after 2007
292 is linked to the thinning of the Beaufort ice cover (Fig. 2), making it more vulnerable
293 to atmospheric forcing during winter.

294 *3.3.2 Changes in ice conditions*

295 Changes in the dynamic properties of sea ice are generally attributed to changes
296 in concentration and thickness, which in turn affect the strength of the ice (Zhang et al.,
297 2012). In sea ice models, including neXtSIM, ice strength is parameterized as a function
298 of ice thickness and concentration (Hibler, 1979). Therefore, we expect the simulated de-
299 cline in ice thickness (Fig. 2b) to weaken the ice pack and reduce the internal ice stress.
300 As a result, this leads to an overall increase in the simulated deformation rates (Fig. 5b)
301 and increased drift speeds (Fig. 5a) in the Beaufort Sea. The positive trend in sea ice
302 drift speeds is consistent with earlier modelling studies (e.g. Zhang et al., 2012) and ob-
303 servations (e.g. Rampal et al., 2009; Spreen et al., 2011).

304 Comparing the simulated LAF in Fig. 4a to the time series of the mean ice speed
305 and deformation rates (Fig. 5) strongly points to a shift in the dynamic sea ice prop-
306 erties and lead formation dynamics after 2007. Both sea ice drift and deformation rates
307 show a pronounced change in the variability, fluctuating between relatively low and high
308 values mirroring the changes in the LAF. High LAF is associated with high deformation
309 rates and increased ice speed in the Beaufort Sea (Fig. 5a and 5b), exceeding 7 cm s^{-1}
310 during breakup events. It is worth noting that both drift and deformation values remain
311 relatively low for winters without significant breakup, i.e. their baseline values do not
312 seem to change much over the 2000–2018 period. This suggests that individual extreme
313 events can substantially alter the overall trend seen in the data.

314 By plotting the ratio between ice drift to wind speed (Fig. 5c) we see a clear in-
315 crease in the ice drift to wind speed ratio, especially during breakup events. This reflects
316 an increased sensitivity of the Beaufort ice cover to wind forcing during the late 2000s,
317 whereas in the earlier period (e.g. in 2005 when the ice was thicker), there is a larger dis-
318 connect between strong winds and ice drift speeds. Overall, this points to changes in the

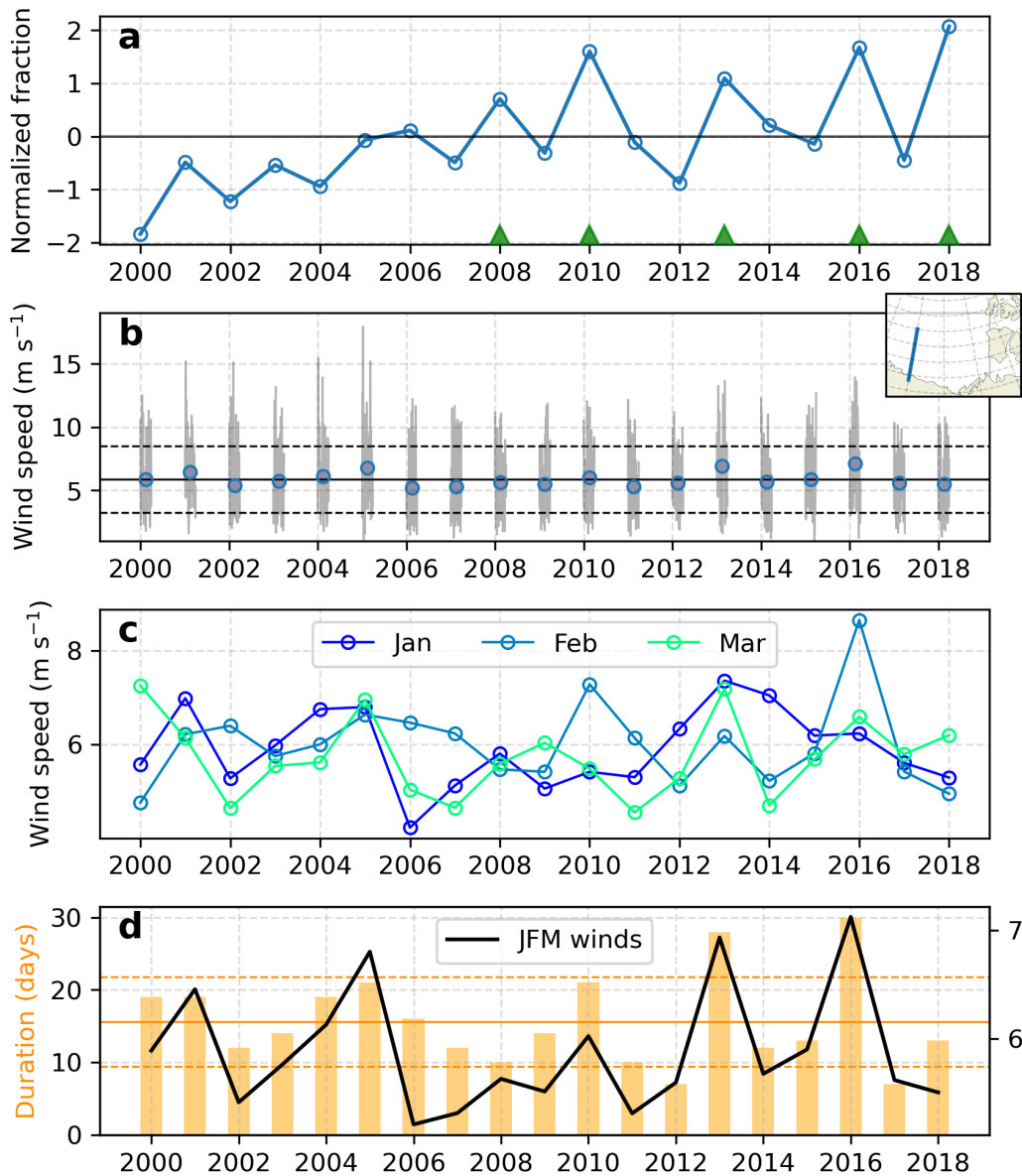


Figure 4. Time series of (a) normalized wintertime lead fraction (%) in Beaufort region, (b) ERA5 daily mean wind speed (m s^{-1}) between $70\text{--}75^\circ\text{N}$ along 150° . The January–March average wind speed is highlighted by blue circles. (c) Monthly mean wind speed for January, February and March. (d) The number of days where the daily wind speed exceeds 8.5 m s^{-1} (one standard deviation above the mean) is shown in bars. Its mean and standard deviation is shown by solid and dashed lines. The solid black line shows the wintertime (January through March) mean wind speed. The time series in (a) is normalized by subtracting its mean and dividing by its standard deviation. The transect used for calculating the winds is indicated in Figure 4b.

319 material properties of sea ice being a major factor in driving the shift we see in the sim-
 320 ulated lead area fraction.

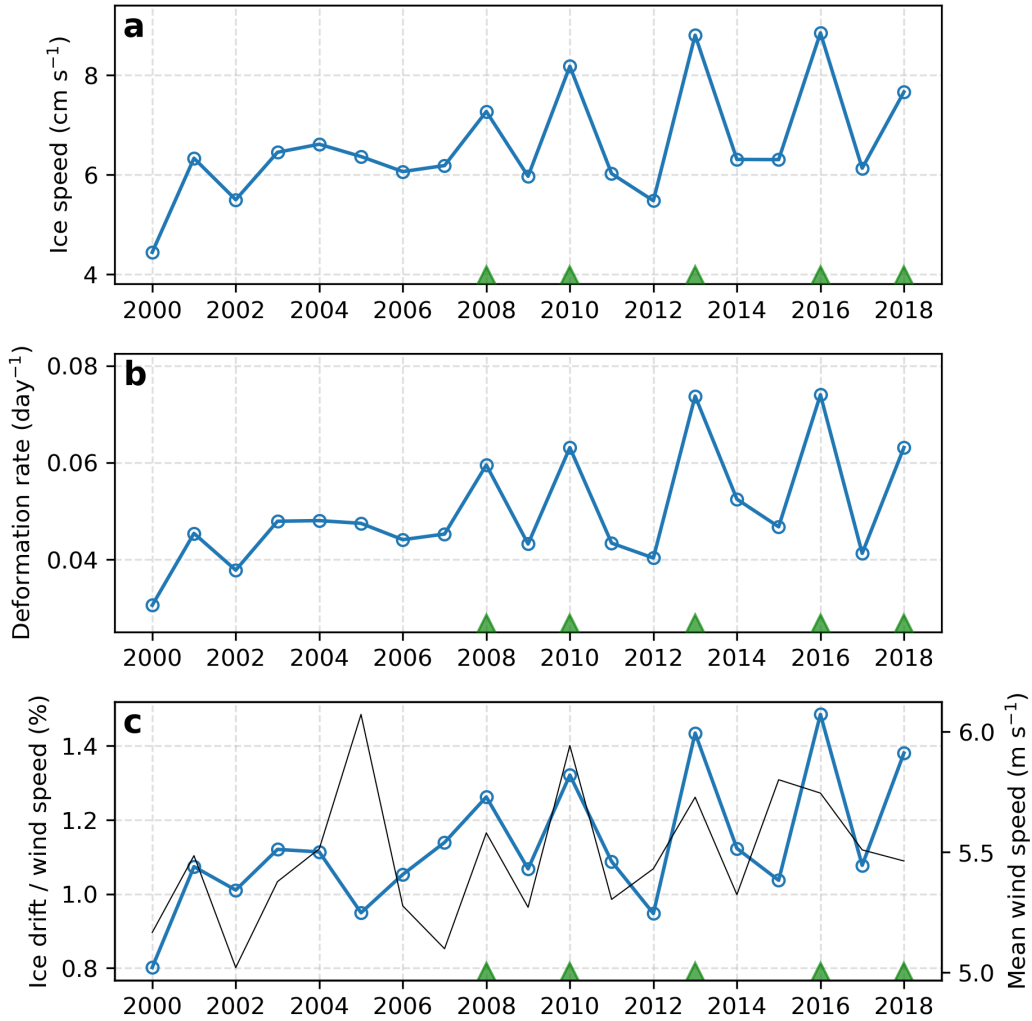


Figure 5. Time series of (a) mean ice speed (cm s^{-1}), (b) total deformation rate ($1/\text{day}$) and (c) ratio (%) between mean sea-ice drift and mean wind speed. The thin black line shows the average wind speed. All time series are based on wintertime (January through March) means and averaged over the Beaufort region. The area used for averaging is shown in Fig. 2. Green triangles highlight winters with significant breakup identified in Figure 3a.

321 **3.4 Impacts on Beaufort ice volume and MYI**

322 In this section, we seek to understand how winter sea ice breakup impacts the ice
 323 volume in the Beaufort Sea. Changes in regional ice volume during winter can be sep-

324 arated into two terms: (i) thermodynamic ice growth and (ii) sea ice transport. Note
 325 that we are omitting the term associated with sea ice melting as this can be considered
 326 negligible during winter (Graham et al., 2019).

327 **3.4.1 Thermodynamic ice growth in leads**

328 In winter, the opening of leads results in intense heat loss from the underlying ocean
 329 and promotes new ice formation. More sea ice breakup could therefore increase the lo-
 330 cal winter ice growth overall and modulate the composition of the Beaufort ice pack by
 331 increasing the fraction of thinner and younger ice types.

332 The thermodynamic ice growth from January through March is shown in Fig. 6
 333 for leads and pack ice, respectively, where growth in leads is associated with the forma-
 334 tion of new and thin sea ice (Rheinländer et al., 2022). Note that the ice growth in leads
 335 is independent of the lead detection algorithm. Overall, the growth of new ice in leads
 336 is increasing over the period 2000–2018 (Fig. 6b). We find a statistically significant lin-
 337 ear trend of 4% per decade for wintertime ice production in leads. This is consistent with
 338 the results of Boutin et al. (2023), who used the same model to find a 4.3% per decade
 339 trend on the pan-Arctic scale. Our result is also consistent with the simulated trend in
 340 LAF (4.2%; Supplementary Fig. S1) and suggests that leads play an increasingly key role
 341 in the local sea-ice volume budget as the ice cover becomes thinner and more fractured.

342 By comparing the growth estimates to the LAF time series in Figure 3a, we see that
 343 winters with more breakups also have larger ice production overall. New ice production
 344 in leads is consistently higher for these years (top 5) compared to the climatology, and
 345 the fraction relative to the total growth is above 40% (except for 2008). Overall, these
 346 results show that winter breakup can significantly increase the local ice volume by en-
 347 hancing ice growth.

348 **3.4.2 Volume transports**

349 The simulated winter-mean ice volume fluxes are shown in Fig. 7 across the Beau-
 350 fort Sea’s eastern, northern and western gates. The transport has been separated into
 351 FYI and MYI contributions. The western gate captures primarily the ice export from
 352 the central Beaufort to the Chukchi Sea, whereas the northern and eastern gate captures
 353 the import of thicker and older sea ice from the Canadian Archipelago and the LIA. This

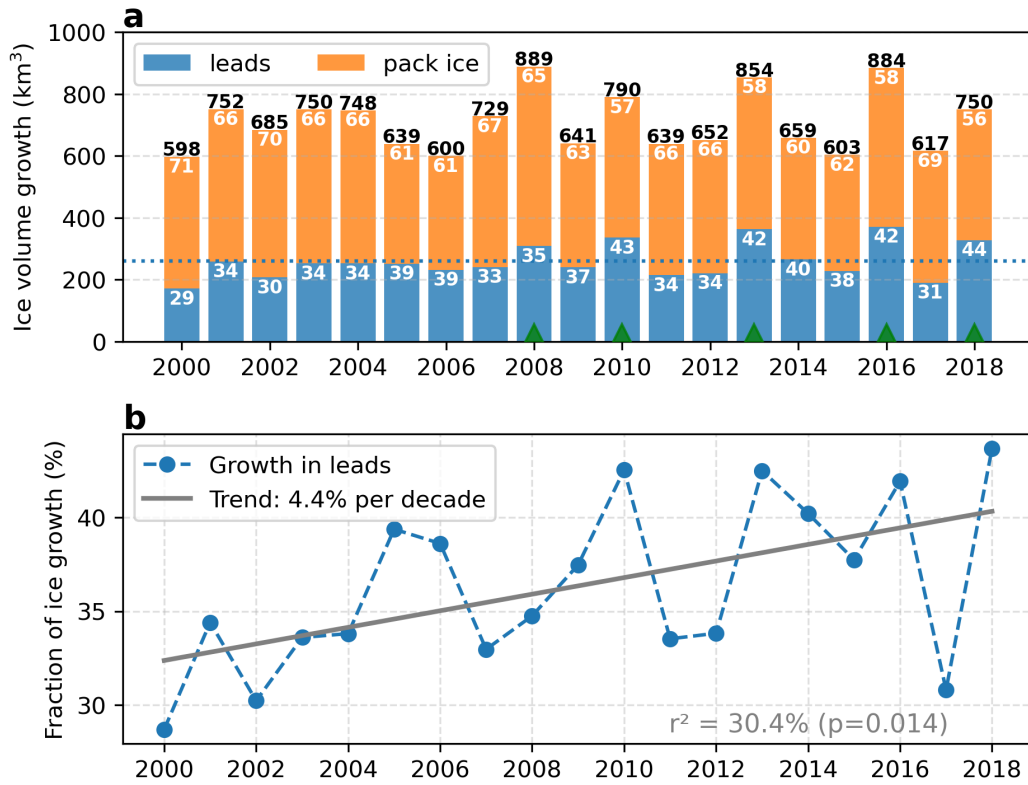


Figure 6. (a) Thermodynamic sea-ice growth (km³) in leads (blue) and pack ice (orange) in the Beaufort Sea during winter (January–March). The dashed line shows the winter climatological mean ice volume growth in leads. Numbers in white indicate the fraction (in %) of the respective growth relative to the total growth (shown by black numbers above the bars). (b) Fraction of ice volume growth in leads relative to the total thermodynamic growth. A linear regression model has been fitted to the data and is shown by the grey line. Breakup years are highlighted by green triangles in (a).

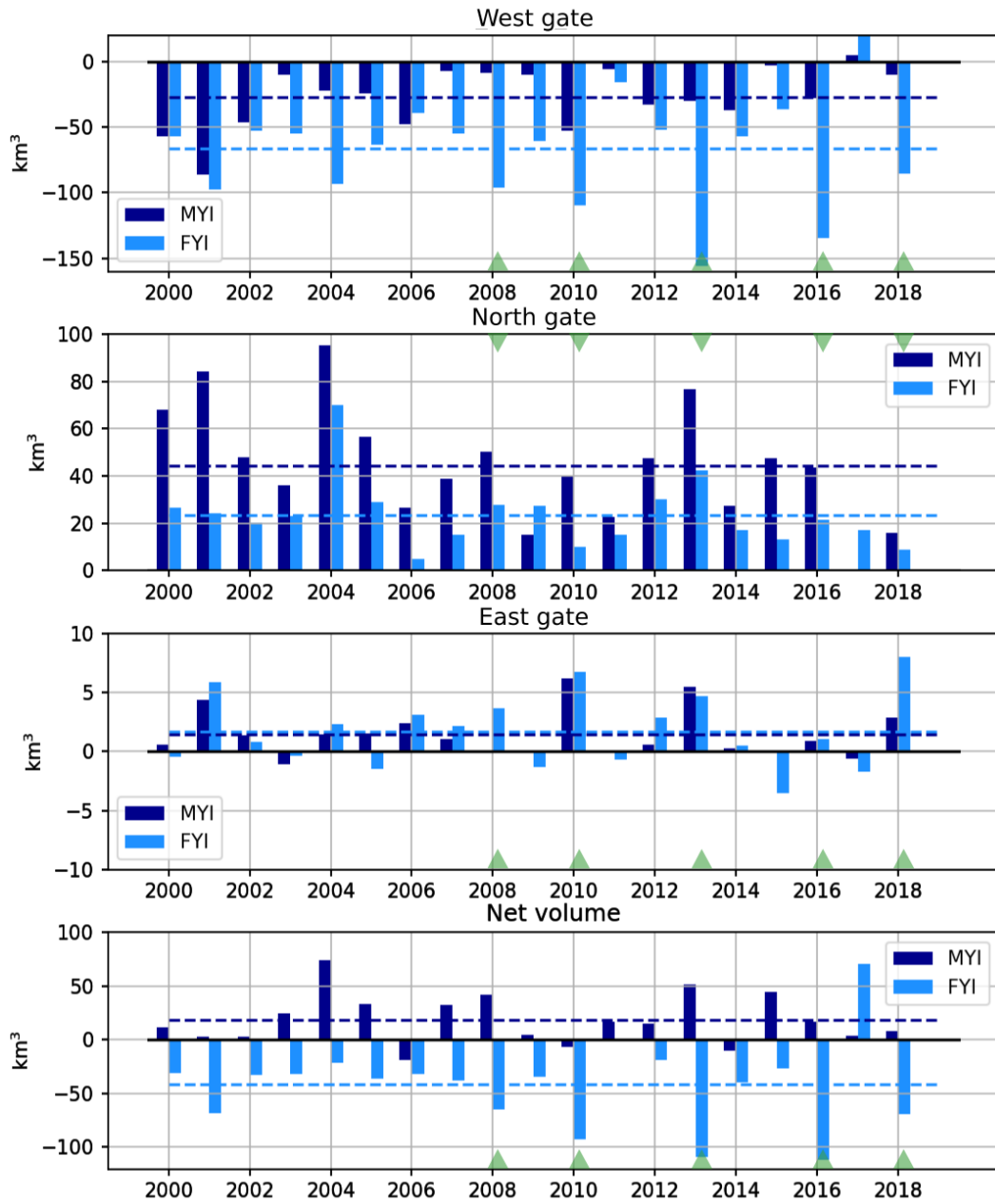


Figure 7. Time series of January–March ice volume fluxes (km^3) into the Beaufort Sea across the eastern (160°W), northern (78°N), and western gates (120°W) and the total fluxes in the bottom panel. The transport is separated into contributions from FYI (light blue) and MYI (dark blue), with dashed lines showing the winter-mean climatologies. Positive values indicate sea ice transport into the Beaufort region.

354 circulation pattern is associated with the anti-cyclonic circulation of the Beaufort Gyre
355 (Howell et al., 2016). Overall, the total fluxes from January through March show a net
356 import of MYI and a net export of FYI. The majority of the transport occurs at the north-
357 ern and western gates, while the transport through the eastern gate is generally small
358 (only accounting for about 6% of the total import).

359 During winters with enhanced lead activity, the ice transport through the Beau-
360 fort region increases (bottom panel in Fig. 7) and is consistent with the higher mean ice
361 drift speeds seen in Fig. 5a. At the western gate, there is a large export of primarily thin-
362 ner and younger FYI during breakup events. A smaller fraction of MYI is also exported,
363 especially in the early 2000s, but is reduced during the later part of the simulation in
364 line with previous studies (e.g. Howell et al., 2016; Babb et al., 2022).

365 At the northern gate, the simulated volume transports are primarily dominated by
366 the import of MYI from the central Arctic. There is generally a higher MYI transport
367 into the Beaufort Sea during breakup events, for example, in 2013 which shows a net im-
368 port of 85 km^3 across the eastern and northern gates. In comparison, the average MYI
369 import is $\sim 45 \text{ km}^3$ over the period 2000–2018. However, years with relatively low lead
370 fractions (in the early 2000s and in 2015) also show high MYI import (and export), while
371 the breakup events in 2016 and 2018 have lower MYI fluxes despite high lead fractions.
372 A possible explanation is that there is simply less MYI in the Arctic in total and, there-
373 fore, less to be transported into the Beaufort region (Babb et al., 2022). This is likely
374 the case in this simulation, which underestimates MYI extent in 2017 and 2018 partly
375 due to unrealistically high melting in the summer of 2016.

376 In total, ice export is larger than import during winter breakup events, which sug-
377 gests that sea ice breakup contributes to regional dynamic ice loss in the short term. This
378 will likely also affect ice transport in the following months and impact the regional ice
379 volume before the beginning of the next melt season. For example, winter export from
380 the Beaufort region could lead to enhanced flushing of MYI through the Beaufort Sea
381 (e.g. Babb et al., 2019) providing dynamical replenishment for the ice loss during win-
382 ter.

383 To understand the cumulative effects of winter breakups, we look at the transport
384 into the Beaufort Sea through the entire cool season from January through June in Fig-
385 ure 8. The 2000–2018 climatology shows a net ice export at the end of the cool season

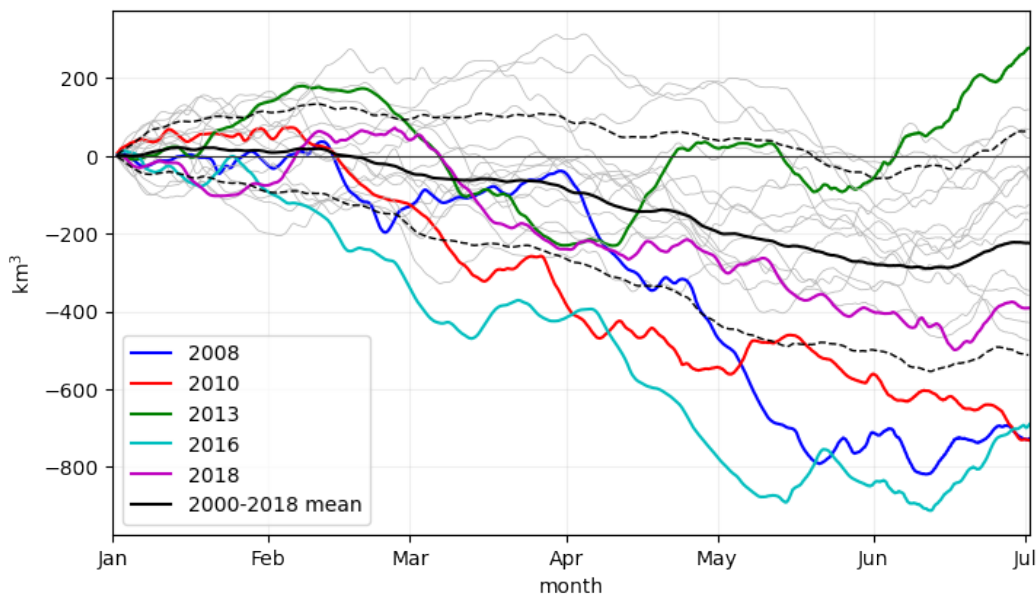


Figure 8. Cumulative sea ice volume fluxes from January to June for all years from 2000 to 2018. Years with high wintertime lead fractions (2008, 2010, 2013, 2016 and 2018) are shown in colours. The 2000–2018 climatology is shown in black with the ± 1 standard deviation.

386 (about -200 km^3 in June). Years with higher lead activity in winter (2008, 2010, 2016,
 387 2018) exhibit larger cumulative net ice export (more than one standard deviation be-
 388 low the mean). A notable exception is 2013, which shows as net ice import, despite a
 389 large export in February–March (Babb et al., 2019; Rheinländer et al., 2022). This was
 390 caused by enhanced advection of thicker MYI through the northern boundary from mid-
 391 April (Fig. 9) offsetting ice export (primarily thin FYI) at the western boundary. Mean-
 392 while, the other breakup events show little evidence of MYI flushing associated with the
 393 increased winter ice export from the Beaufort Sea.

394 Overall, these results suggest that winter breakup events may have a negative im-
 395 pact on the Beaufort ice mass balance by enhancing ice export, despite also promoting
 396 significant new ice growth. But what is the combined effect of winter breakup on the Beau-
 397 fort ice volume? In Figure 10, we show the relationship between wintertime lead area
 398 fraction, i.e. over the period from January through March, and the ice conditions in the
 399 Beaufort Sea at the end of the cool season (from January 1 to June 1). The cumulative
 400 cool season transport out of the Beaufort Sea is generally larger when the LAF is high
 401 and we see a clear separation of the breakup years that also have enhanced export. The

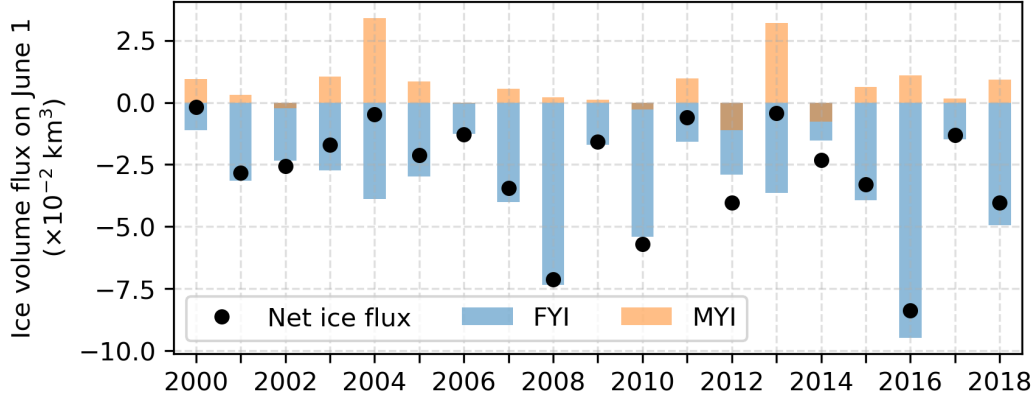


Figure 9. June 1 cumulative ice volume fluxes separated into FYI (blue) and MYI (orange) contributions from 2000 to 2018 in the Beaufort region. The net June 1 ice volume flux is shown by black circles. Positive (negative) values corresponds to a net import (export).

402 correlation between cool season transport and the Beaufort ice volume at the beginning
 403 of June exhibits a similar grouping, with breakup years showing lower ice volume val-
 404 ues on June 1. A similar relationship was also found based on satellite observations (e.g.
 405 Babb et al., 2019; Moore et al., 2022), suggesting that high winter export from the Beau-
 406 fort Sea results in an anomalously thin ice cover and negative regional volume anoma-
 407 lies. This could preconditioning the ice cover for increased summer melt and ultimately
 408 result in record low regional September sea ice minima as shown by Babb et al. (2019).

409 **4 Discussion**

410 In an earlier modelling study, Wang et al. (2016) simulated the time evolution of
 411 lead formation in the Beaufort Sea over the last three decades (1985–2014) using a high-
 412 resolution (4.5 km) sea-ice model (Finite Element Sea Ice-Ocean Model; FESOM). In
 413 contrast to the neXtSIM simulation, they observed no increase in the number of large-
 414 scale breakup events in winter, which they related to the absence of wind stress trends
 415 in the Beaufort region. However, one of the notable contrasts between these two mod-
 416 els is the difference in sea ice rheology; m-EVP for FESOM versus BBM in neXtSIM.
 417 This could lead to significant differences in how the ice cover responds dynamically to
 418 changes in the mechanical ice properties and the sensitivity to wind forcing. Another dif-
 419 ference is the definition of leads in Wang et al. (2016), which are defined as locations where
 420 the sea ice is at least 20% thinner than at its surroundings (within a 25-km radius). Firstly,

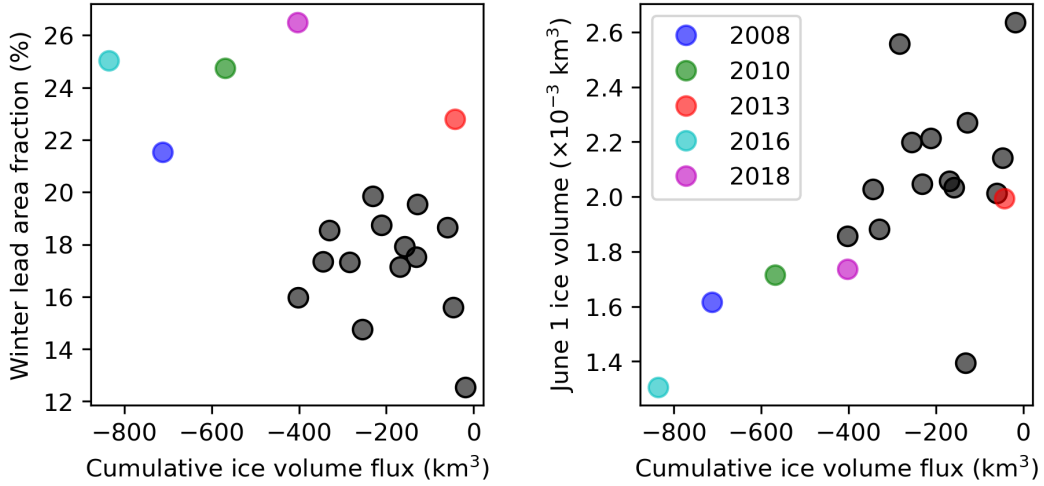


Figure 10. Scatterplot of the cool season (January 1 - June 1) ice volume flux and (a) winter mean (January–March) lead area fraction and (b) June 1 ice volume. Breakup years (2008, 2010, 2013, 2016 and 2018) are highlighted in colours.

421 this excludes very wide leads, and secondly may fail to capture very localized divergence
 422 events leading to drops in sea ice concentration as seen in the neXtSIM simulation. Mean-
 423 while, recent observational data based on MODIS imagery (Willmes et al., 2023) show
 424 a significant positive trend of 2% per decade in lead frequencies in the Beaufort Sea over
 425 the period from 2002 to 2021 (during April only). This is similar to Hoffman et al. (2022)
 426 who observed a small, but significant increase in pan-Arctic leads from satellite data over
 427 the same period, despite large uncertainty due to the increasing cloud cover in the Arc-
 428 tic.

429 We find that the change in lead formation dynamics simulated by the neXtSIM model,
 430 notably the increased variability in lead formation after 2007, can be linked to a shift
 431 in the Beaufort ice dynamics. Such transitions have been reported in observations. Long-
 432 term sea ice data from satellites dating back to the 1980s show evidence that the Beau-
 433 fort Sea transitioned to a thinner state in 1998 (Hutchings & Rigor, 2012 and Fig. 1 in
 434 Babb et al., 2019). Another transition occurred around 2007 (e.g. Moore et al., 2022;
 435 Babb et al., 2022), which reflected a shift from an old ice regime (1979–2007) when the
 436 region was dominated by MYI to a young ice regime (2007–present). Similarly, Wood
 437 et al. (2013) pointed to a “new normal” climate in the Beaufort Sea since 2007, char-

acterized by an increasingly mobile and thus more dynamic ice pack, which agrees with the increase in ice drift in Figure 2c.

Our results indicate, that sea ice thinning and loss of MYI in the Beaufort region makes the ice cover less resilient to wind forcing thus increasing the likelihood of large breakups. This could lead to enhanced inter-annual variability in Beaufort Sea ice conditions and may increase the potential for rapid sea ice loss (Moore et al., 2022; Maslanik et al., 2007). Similarly, Petty et al. (2016) found an amplified sensitivity of the Beaufort sea ice circulation in winter to wind forcing during the late-2000s. This increase in winter ice drift is commonly attributed to general sea ice thinning and reduction in mechanical ice strength (Zhang et al., 2012; Rampal et al., 2009), which is also evident from our results in Fig. 5. Meanwhile, Jewell and Hutchings (2023) noted that changes in ice thickness is not the only factor controlling breakup. Atmospheric conditions such as wind direction, storm propagation and duration of strong winds are also important factors that contribute to sea-ice breakup. In fact, the LAF timeseries in Figure 3 show that breakup events also occurred during the early-2000s (for example in 2005 and 2006) when the ice was considerably thicker. This emphasises the importance of atmospheric forcing in initiating breakup.

While the atmosphere plays a dominant role in triggering sea-ice breakup on short time scales (days to weeks), the ocean may also play a role in preconditioning sea-ice breakup on seasonal time scales (Willmes et al., 2023). For example, enhanced ocean heat fluxes during summer and autumn may predispose the ice cover to enhanced melt, resulting in a thinner and weaker ice cover before the beginning of the cooling season (Herbaut et al., 2022; Graham et al., 2019). Lead formation can also be expected to have significant impacts on the ocean underneath, for example by enhancing mechanical energy input available for mixing and through brine formation thereby affecting mixed layer properties and halocline stability (Matsumura & Hasumi, 2008; Peralta-Ferriz & Woodgate, 2015; Shimada et al., 2005). Mixing up warmer waters through lead opening could enhance basal melting and limit new ice growth in the leads (e.g. Graham et al., 2019). Such feedbacks could be important for ice-ocean interactions even on longer time scales but they are not assessed explicitly in this study.

5 Summary and conclusions

This paper presents a multi-decadal simulation using the coupled ocean-sea-ice neXtSIM-OPA model and investigates the temporal changes in wintertime sea ice leads in the Beaufort Sea and their impacts. The simulation shows a small but significant increasing trend in the Beaufort lead area fraction (4% per decade) over the winter season (January through March) for the period 2000 to 2018. This is consistent with a general decrease in ice thickness and MYI cover as well as enhanced drift speeds during winter in the Beaufort region.

Around 2007 we find a notable increase in the simulated lead area fraction variability associated with enhanced sea ice breakup, high deformation rates and an increase in the mean ice velocities. These changes coincide with the observed regime shift that occurred in the Beaufort Sea in 2007 (Wood et al., 2013; Moore et al., 2022), characterized by a transition from a state dominated by thicker and older MYI towards more seasonal, thinner and younger sea ice. We find no significant trend in the surface winds during winter over the simulated time period. This suggests that the changes in lead formation dynamics can be attributed to changes in the sea ice conditions (i.e. thinning, loss of ice strength and enhanced deformation) rather than changes in the atmospheric forcing. Consequently, the ice cover becomes more sensitive to wind forcing, which may lead to enhanced inter-annual variability in Beaufort Sea ice conditions and more extreme breakup during winter.

Several large breakup events are identified which significantly impact the regional thermodynamic ice production, with new ice growth in leads contributing up to 40% of the total winter ice growth. This implies that sea ice leads play an important role in the local ice mass balance in the Arctic (as Boutin et al., 2023, also found). Meanwhile, years with high lead activity in winter consistently exhibit increased ice export, primarily FYI, from the Beaufort Sea throughout the entire cool season (January 1 to June 1). While some breakup events also show an enhanced import of MYI to the Beaufort from the central Arctic (e.g. in 2013), we find no consistent evidence that winter breakup leads to the flushing of MYI through the Beaufort Sea.

Overall, these results suggest that winter breakups have a negative impact on the Beaufort ice volume, preconditioning a thinner and weaker ice pack at the end of the cool season (see also Babb et al., 2016, 2019; Moore et al., 2022). This could lead to earlier

500 breakup in spring and enhanced summer melt, thereby contributing to accelerating sea
 501 ice loss in the Beaufort Sea. This further highlights the need to include small-scale sea-
 502 ice deformation and fracturing in global climate models to accurately simulate future Arc-
 503 tic sea-ice mass balance, particularly the evolution of MYI in the Arctic.

504 **Data Availability Statement**

505 The output from the neXtSIM-OPA simulation is available as NetCDF files at <https://doi.org/10.5281/Zenodo.7277523>. Jupyter Notebooks for data analysis and plotting
 506 are located in a public GitHub repository at <https://zenodo.org/badge/latestdoi/682991902>. The ERA-5 data was downloaded from the Copernicus Climate Change Ser-
 507 vice Climate Data Store (C3S) <https://cds.climate.copernicus.eu/cdsapp#!/dataset/reanalysis-era5-single-levels?tab=overview>.
 508
 509
 510

511 **Acknowledgments**

512 This work was supported by the Bjerknes Centre for Climate Research. The authors would
 513 like to acknowledge the support of the Norwegian Research Council Grant Number 302934:
 514 *Atmosphere-Sea Ice interactions in the new Arctic*. A special thanks to the organizers
 515 and participants of the Beaufort Gyre workshop in Woods Hole, March 2023, which helped
 516 inspire this work.

517 **References**

- 518 Assmy, P., Fernández-Méndez, M., Duarte, P., Meyer, A., Randelhoff, A., Mundy,
 519 C. J., ... Granskog, M. A. (2017, jan). Leads in Arctic pack ice enable early
 520 phytoplankton blooms below snow-covered sea ice. *Scientific Reports 2017 7:1*,
 521 7(1), 1–9. doi: 10.1038/srep40850
- 522 Babb, D. G., Galley, R. J., Barber, D. G., & Rysgaard, S. (2016, jan). Phys-
 523 ical processes contributing to an ice free Beaufort Sea during September
 524 2012. *Journal of Geophysical Research: Oceans*, 121(1), 267–283. doi:
 525 10.1002/2015JC010756
- 526 Babb, D. G., Galley, R. J., Howell, S. E., Landy, J. C., Stroeve, J. C., & Barber,
 527 D. G. (2022, may). Increasing Multiyear Sea Ice Loss in the Beaufort Sea: A
 528 New Export Pathway for the Diminishing Multiyear Ice Cover of the Arctic
 529 Ocean. *Geophysical Research Letters*, 49(9). doi: 10.1029/2021GL097595

- 530 Babb, D. G., Landy, J. C., Barber, D. G., & Galley, R. J. (2019, sep). Winter Sea
 531 Ice Export From the Beaufort Sea as a Preconditioning Mechanism for En-
 532 hanced Summer Melt: A Case Study of 2016. *Journal of Geophysical Research:*
 533 *Oceans*, *124*(9), 6575–6600. doi: 10.1029/2019JC015053
- 534 Beitsch, A., Kaleschke, L., & Kern, S. (2014). Investigating High-Resolution AMSR2
 535 Sea Ice Concentrations during the February 2013 Fracture Event in the Beau-
 536 fort Sea. *Remote Sens*, *6*, 6. doi: 10.3390/rs6053841
- 537 Bouchat, A., Hutter, N., Chanut, J., Dupont, F., Dukhovskoy, D., Garric, G., ...
 538 Wang, Q. (2022, apr). Sea Ice Rheology Experiment (SIREx): 1. Scaling and
 539 Statistical Properties of Sea-Ice Deformation Fields. *Journal of Geophysical*
 540 *Research: Oceans*, *127*(4), e2021JC017667. doi: 10.1029/2021JC017667
- 541 Bouillon, S., & Rampal, P. (2015). Presentation of the dynamical core of neXtSIM, a
 542 new sea ice model. *Ocean Modelling*, *91*, 23–37. doi: 10.1016/j.ocemod.2015.04
 543 .005
- 544 Boutin, G., Ólason, E., Rampal, P., Regan, H., Lique, C., Talandier, C., ... Ricker,
 545 R. (2023, feb). Arctic sea ice mass balance in a new coupled ice-ocean
 546 model using a brittle rheology framework. *Cryosphere*, *17*(2), 617–638. doi:
 547 10.5194/TC-17-617-2023
- 548 Fadeev, E., Rogge, A., Ramondenc, S., Nöthig, E. M., Wekerle, C., Bienhold, C., ...
 549 Iversen, M. H. (2021, nov). Sea ice presence is linked to higher carbon export
 550 and vertical microbial connectivity in the Eurasian Arctic Ocean. *Communica-*
 551 *tions Biology* *2021 4:1*, *4*(1), 1–13. doi: 10.1038/s42003-021-02776-w
- 552 Graham, R. M., Itkin, P., Meyer, A., Sundfjord, A., Spreen, G., Smedsrud, L. H., ...
 553 Granskog, M. A. (2019, dec). Winter storms accelerate the demise of sea ice
 554 in the Atlantic sector of the Arctic Ocean. *Scientific Reports*, *9*(1), 1–16. doi:
 555 10.1038/s41598-019-45574-5
- 556 Heil, P., & Hibler, W. D. (2002). Modeling the high-frequency component of
 557 arctic sea ice drift and deformation. *Journal of Physical Oceanography*,
 558 *32*, 3039–3057. doi: [https://doi.org/10.1175/1520-0485\(2002\)032<3039:](https://doi.org/10.1175/1520-0485(2002)032<3039:MTHFCO>2.0.CO;2)
 559 [MTHFCO>2.0.CO;2](https://doi.org/10.1175/1520-0485(2002)032<3039:MTHFCO>2.0.CO;2)
- 560 Herbaut, C., Houssais, M. N., Blaizot, A. C., & Molines, J. M. (2022, jun). A
 561 Role for the Ocean in the Winter Sea Ice Distribution North of Svalbard.
 562 *Journal of Geophysical Research: Oceans*, *127*(6), e2021JC017852. doi:

- 563 10.1029/2021JC017852
- 564 Hibler, W. D. (1979). A Dynamic Thermodynamic Sea Ice Model. *JPO*, 9(4), 815–
565 846. doi: 10.1175/1520-0485(1979)009
- 566 Hoffman, J. P., Ackerman, S. A., Liu, Y., & Key, J. R. (2022, nov). A 20-Year
567 Climatology of Sea Ice Leads Detected in Infrared Satellite Imagery Using a
568 Convolutional Neural Network. *Remote Sensing 2022, Vol. 14, Page 5763*,
569 14(22), 5763. doi: 10.3390/RS14225763
- 570 Howell, S. E. L., Brady, M., Derksen, C., & Kelly, R. E. J. (2016, apr). Re-
571 cent changes in sea ice area flux through the Beaufort Sea during the sum-
572 mer. *Journal of Geophysical Research: Oceans*, 121(4), 2659–2672. doi:
573 10.1002/2015JC011464
- 574 Hutchings, J. K., & Rigor, I. G. (2012, aug). Role of ice dynamics in anomalous
575 ice conditions in the Beaufort Sea during 2006 and 2007. *Journal of Geophysi-
576 cal Research: Oceans*, 117(C8), 0–04. doi: 10.1029/2011JC007182
- 577 Hutter, N., Bouchat, A., Dupont, F., Dukhovskoy, D., Koldunov, N., Lee, Y. J.,
578 ... Wang, Q. (2022, apr). Sea Ice Rheology Experiment (SIREx): 2. Eval-
579 uating Linear Kinematic Features in High-Resolution Sea Ice Simulations.
580 *Journal of Geophysical Research: Oceans*, 127(4), e2021JC017666. doi:
581 10.1029/2021JC017666
- 582 Jewell, M. E., & Hutchings, J. K. (2023, jan). Observational Perspectives on Beau-
583 fort Sea Ice Breakouts. *Geophysical Research Letters*, 50(1), e2022GL101408.
584 doi: 10.1029/2022GL101408
- 585 Kwok, R. (2006, nov). Contrasts in sea ice deformation and production in the Arc-
586 tic seasonal and perennial ice zones. *Journal of Geophysical Research: Oceans*,
587 111(C11), 11–22. doi: 10.1029/2005JC003246
- 588 Kwok, R. (2018, oct). *Arctic sea ice thickness, volume, and multiyear ice cover-
589 age: Losses and coupled variability (1958-2018)* (Vol. 13) (No. 10). Institute of
590 Physics Publishing. doi: 10.1088/1748-9326/aae3ec
- 591 Kwok, R., & Cunningham, G. F. (2010, oct). Contribution of melt in the Beaufort
592 Sea to the decline in Arctic multiyear sea ice coverage: 1993-2009. *Geophysical
593 Research Letters*, 37(20). doi: 10.1029/2010GL044678
- 594 Lewis, B. J., & Hutchings, J. K. (2019, may). Leads and Associated Sea Ice Drift in
595 the Beaufort Sea in Winter. *Journal of Geophysical Research: Oceans*, 124(5),

- 596 3411–3427. doi: 10.1029/2018JC014898
- 597 Madec, G. (2008). *NEMO ocean engine, Note du Pôle de modélisation* (Tech. Rep.).
 598 Institut Pierre-Simon Laplace (IPSL), France, No 27.
- 599 Maslanik, J. A., Fowler, C., Stroeve, J., Drobot, S., Zwally, J., Yi, D., & Emery,
 600 W. (2007, dec). A younger, thinner Arctic ice cover: Increased potential for
 601 rapid, extensive sea-ice loss. *Geophysical Research Letters*, *34*(24), 24501. doi:
 602 10.1029/2007GL032043
- 603 Matsumura, Y., & Hasumi, H. (2008, jan). Brine-Driven Eddies under Sea Ice
 604 Leads and Their Impact on the Arctic Ocean Mixed Layer. *Journal of Physical*
 605 *Oceanography*, *38*(1), 146–163. doi: 10.1175/2007JPO3620.1
- 606 Moore, G., Steele, M., Schweiger, A. J., Zhang, J., & Laidre, K. L. (2022, aug).
 607 Thick and old sea ice in the Beaufort Sea during summer 2020/21 was associ-
 608 ated with enhanced transport. *Communications Earth and Environment*, *3*(1),
 609 1–11. doi: 10.1038/s43247-022-00530-6
- 610 Ólason, E., Boutin, G., Korosov, A., Rampal, P., Williams, T., Kimmritz, M., . . .
 611 Samaké, A. (2022, jul). A new brittle rheology and numerical framework for
 612 large-scale sea-ice models. *Journal of Advances in Modeling Earth Systems*,
 613 e2021MS002685. doi: 10.1029/2021MS002685
- 614 Peralta-Ferriz, C., & Woodgate, R. A. (2015, may). Seasonal and interannual
 615 variability of pan-Arctic surface mixed layer properties from 1979 to 2012
 616 from hydrographic data, and the dominance of stratification for multiyear
 617 mixed layer depth shoaling. *Progress in Oceanography*, *134*, 19–53. doi:
 618 10.1016/J.POCEAN.2014.12.005
- 619 Petty, A. A., Hutchings, J. K., Richter-Menge, J. A., & Tschudi, M. A. (2016). Sea
 620 ice circulation around the Beaufort Gyre: The changing role of wind forcing
 621 and the sea ice state. *Journal of Geophysical Research: Oceans*, *121*, 3278–
 622 3296. doi: 10.1002/2015JC010903
- 623 Rampal, P., Bouillon, S., Ólason, E., & Morlighem, M. (2016, may). NeXtSIM: A
 624 new Lagrangian sea ice model. *Cryosphere*, *10*(3), 1055–1073. doi: 10.5194/tc
 625 -10-1055-2016
- 626 Rampal, P., Dansereau, V., Olason, E., Bouillon, S., Williams, T., Korosov, A., &
 627 Samaké, A. (2019, sep). On the multi-fractal scaling properties of sea ice
 628 deformation. *Cryosphere*, *13*(9), 2457–2474. doi: 10.5194/tc-13-2457-2019

- 629 Rampal, P., Weiss, J., & Marsan, D. (2009, may). Positive trend in the mean speed
630 and deformation rate of Arctic sea ice, 1979–2007. *Journal of Geophysical Re-*
631 *search*, *114*(C5), C05013. doi: 10.1029/2008JC005066
- 632 Regan, H., Rampal, P., Ólason, E., Boutin, G., & Korosov, A. (2023, may).
633 Modelling the evolution of Arctic multiyear sea ice over 2000–2018. *The*
634 *Cryosphere*, *17*(5), 1873–1893. doi: 10.5194/TC-17-1873-2023
- 635 Rheinländer, J. W., Davy, R., Ólason, E., Rampal, P., Spensberger, C., Williams,
636 T. D., . . . Spengler, T. (2022, jun). Driving Mechanisms of an Extreme Winter
637 Sea Ice Breakup Event in the Beaufort Sea. *Geophysical Research Letters*,
638 *49*(12). doi: 10.1029/2022GL099024
- 639 Richter-Menge, J. A., & Farrell, S. L. (2013, nov). Arctic sea ice conditions in spring
640 2009–2013 prior to melt. *Geophysical Research Letters*, *40*(22), 5888–5893. doi:
641 10.1002/2013GL058011
- 642 Ricker, R., Kauker, F., Schweiger, A., Hendricks, S., Zhang, J., & Paul, S. (2021,
643 jul). Evidence for an Increasing Role of Ocean Heat in Arctic Winter
644 Sea Ice Growth. *Journal of Climate*, *34*(13), 5215–5227. doi: 10.1175/
645 JCLI-D-20-0848.1
- 646 Shimada, K., Itoh, M., Nishino, S., McLaughlin, F., Carmack, E., & Proshutinsky,
647 A. (2005, feb). Halocline structure in the Canada Basin of the Arctic Ocean.
648 *Geophysical Research Letters*, *32*(3), 1–5. doi: 10.1029/2004GL021358
- 649 Spreen, G., Kwok, R., & Menemenlis, D. (2011, oct). Trends in Arctic sea ice drift
650 and role of wind forcing: 1992–2009. *Geophysical Research Letters*, *38*(19),
651 n/a–n/a. doi: 10.1029/2011GL048970
- 652 Spreen, G., Kwok, R., Menemenlis, D., & Nguyen, A. T. (2017, jul). Sea-ice defor-
653 mation in a coupled ocean–sea-ice model and in satellite remote sensing data.
654 *The Cryosphere*, *11*(4), 1553–1573. doi: 10.5194/tc-11-1553-2017
- 655 Talandier, C., & Lique, C. (2021, dec). CREG025.L75-NEMOr3.6.0: Source code as
656 input files required to perform a CREG025.L75 experiment that relies on the
657 NEMO release 3.6. *Zenodo [code]*. doi: 10.5281/ZENODO.5802028
- 658 Wang, Q., Danilov, S., Jung, T., Kaleschke, L., & Wernecke, A. (2016, jul).
659 Sea ice leads in the Arctic Ocean: Model assessment, interannual variabil-
660 ity and trends. *Geophysical Research Letters*, *43*(13), 7019–7027. doi:
661 10.1002/2016GL068696

- 662 Williams, J., Tremblay, B., Newton, R., & Allard, R. (2016, aug). Dynamic Pre-
663 conditioning of the Minimum September Sea-Ice Extent. *Journal of Climate*,
664 *29*(16), 5879–5891. doi: 10.1175/JCLI-D-15-0515.1
- 665 Willmes, S., Heinemann, G., & Schnaase, F. (2023, aug). Patterns of winter-
666 time Arctic sea-ice leads and their relation to winds and ocean currents. *The*
667 *Cryosphere*, *17*(8), 3291–3308. doi: 10.5194/TC-17-3291-2023
- 668 Winton, M. (2000, apr). A reformulated three-layer sea ice model. *Journal of Atmo-*
669 *spheric and Oceanic Technology*, *17*(4), 525–531. doi: 10.1175/1520-0426(2000)
670 017(0525:ARTLSI)2.0.CO;2
- 671 Wood, K. R., Overland, J. E., Salo, S. A., Bond, N. A., Williams, W. J., & Dong,
672 X. (2013, oct). Is there a “new normal” climate in the Beaufort Sea? *Polar*
673 *Research*, *32*(SUPPL.). doi: 10.3402/POLAR.V32I0.19552
- 674 Zhang, J., Lindsay, R., Schweiger, A., & Rigor, I. (2012, oct). Recent changes in the
675 dynamic properties of declining Arctic sea ice: A model study. *Geophysical Re-*
676 *search Letters*, *39*(20), 2012GL053545. doi: 10.1029/2012GL053545